Optik - International Journal for Light and Electron Optics 220 (2020) 165116

Contents lists available at ScienceDirect

Optik

journal homepage: www.elsevier.com/locate/ijleo

Original research article

SHADE: Absorption spectroscopy enhancement with ambient light estimation and narrow-band detection

Habib Sherkat, Marco Antonio Pinto-Orellana, Peyman Mirtaheri*

Department of Mechanical, Electronics and Chemical Engineering, Faculty of Technology, Art and Design, Oslo Metropolitan University, Oslo, Norway

ARTICLE INFO

Keywords:
Multi-wavelength spectroscopy
Functional near-infrared spectroscopy (fNIRS)
Diffuse optical tomography (DOT)
Ambient light suppression
Optical topography

ABSTRACT

Ambient light (AML) limits the usage of absorption spectroscopy to strictly-controlled environments due to its impact on the quality of the signals. In medical applications for Optical instruments that require high reliability and validity results, it is indispensable to control AML impact. In this work, we present a multi-wavelength optical acquisition method, here called SHADE. The technique increases the quality of the optical signals, dynamically assesses AML, and enables mitigating the AML influence on the data. Our proposed technique involves four primary functions: (1) Multiplexing/demultiplexing of target wavelengths using a frequency-division method; (2) Robust signal recovery using inverse notch filters; (3) Concurrent AML intensity estimation; (4) A simple post-processing (offline) suppression of AML interference. We introduce the mathematical framework of SHADE to demonstrate the theoretical scope and limitations. SHADE was also experimentally tested by using a digital signal processing board under different conditions. The results confirmed the performance of the AML reconstruction and the potential of such a method for further improvements of the signal quality.

1. Introduction

The interaction between light and a specific sample can determine its chemical species due to optical phenomena such as absorption or reflection. The absorption pattern, on different wavelengths of the retrieved light, links to the concentration of the chromophore elements and their spectral signature [1,2]. This identification is known as absorption spectrometry and optical tomography, which has had an increasing interest in healthcare-related applications [3]. Some examples of these applications are monitoring and detection of the brain activity, breast cancer, glucose levels, tissue and joint physiology, vessel occlusion, and muscle activities [4–6,3]. The widespread attention toward these methods is possibly the result of available and affordable narrow-band light sources called light-emitting diodes or abbreviated as LEDs.

However, these optical based devices are vulnerable to ambient light (AML). The AML links to the intensity and spectra of incandescent light, daylight, halogen, and fluorescent lamps. These unwanted light sources are inevitable for the environment illuminate but may have destructive effects such as detector saturation, and varied baseline of the optical spectra. Thus, prevention of the direct detector exposure to the AML is one of the initial considerations in the development of any optical devices. The protection can be as straightforward as embedding the system and the tissue inside a light-proof enclosure. This approach is similar to the design of the pulse oximeters. For monitoring blood's oxygen saturation on the fingertip, the adequacy of this technique is confirmed [7]. However, the size of some spectroscopy devices and body organs (e.g., diffuse optical tomography of the brain) may prevent the total AML removal [8] as the tissue and the detector cannot be covered completely. During movements of portable devices, some AML may

* Corresponding author.
E-mail addresses: Sherkat@oslomet.no (H. Sherkat), Marco.Pinto@oslomet.no (M.A. Pinto-Orellana), Peymanm@oslomet.no (P. Mirtaheri).

https://doi.org/10.1016/j.ijleo.2020.165116
Received 4 April 2020; Accepted 8 June 2020

leak into the optical detector. In this context, AML leakage refers to the stray light that reaches the detector due to the contact surface detachment between the sensor and the skin during sudden movement. The subsequent consequence of AML leakage is the high non-stationary impact on the signal. Moreover, as we argue in Section 4, the non-homogeneous illumination of an environment exacerbates this stochastic characteristic. The non-stationary influence requires a method to actively estimate and cancel out the undesired impact of the AML. Otherwise, AML can modify the optical spectra, which can lead to anomaly and misinterpretations of the physiological signals.

In the laboratory environment, passive methods to counteract the AML issues can fall under some headings including covering by shield-cloth [9,10], limiting the experiment in a dark environment [11], attaching of a reference detector [12], insertion of optical filters inside the system [13], and using polarizers [14,9,10]. These passive techniques will not only complicate the measuring schemes but also do not alleviate the aforementioned non-stationary characteristics of AML, such as AML leakage. Some systems incorporated the estimation of AML during dark periods. A dark period is a time when all the wavelength sources are shut-off, and the amount of light during this period expected to represent the AML [15,16]. Nevertheless, systems, with dark period measurement, suffer from lacking signal enhancement techniques. Narrow-band detection techniques are extensively used in applications to detect a small alternating signal buried in noise. The lack of this technique in portable optical tomography devices makes them further exposed to electrical noise.

Optical tomography devices, such as dynamic diffuse optical tomography, record quasi-dynamic signals [17] that restrict the use of the conventional average because it reduces the system's sampling frequency. The sampling rate should be above the Nyquist rate of the signal bandwidth, and its selection is critical to detect dynamic changes. Therefore, narrow-band detection techniques, which do not decrease the sampling frequency, have had a pivotal role in absorption spectroscopy. This signal enhancement recovers the low-level signal from usual flicker, or "1/f", noise and white noise. The noise suppression is achievable with amplitude modulation of narrow-band light sources, and the following frequency-selective filters, to demodulate the received signal. The joint selection of a modulation technique and an inverse notch filter may influence the selectivity, implementation complexity, and optimal noise reduction [18]. The lock-in-amplification seems to be the most practiced technique in continuous-wave optical tomography devices, particularly in brain-computer interfaces (BCI) based on functional near-infrared spectroscopy (fNIRS) [19–23]. However, this narrow-band detection technique is usually implemented with the trade-off of losing information relating to the measurement of AML [19–23]. To the best of our knowledge, a narrow-band detection technique with a dynamic estimation of AML for multiple wavelength spectroscopy has not been introduced previously.

In this paper, we propose a narrow-band detection technique with dynamic AML estimation. The suggested technique, SHADE, includes frequency-division multiplexing (FDM) to modulate each wavelength of the spectroscopy system and a set of inverse notch filters to recovers them from the noise. This initial structure can be considered as a generalization of the model presented by Masciotti et al. [24]. However, our technique includes an AML estimator, and there are not any restrictions on the required type of inverse notch filter, i.e., SHADE works with any arbitrary inverse notch filters. Such a method can contribute to the advancement of the future fNIRS-based brain-computer interface (BCI) devices.

This paper is organized in the following structure: in Section 2, we explore the mathematical model of our proposed method, SHADE. Then, we present an efficient empirical compensation algorithm to minimize the noise effect. Next, we described the implementation of SHADE on the microcontroller (MCU) of a customized digital signal processing board. In Section 3, we explained the experimental evaluations of the SHADE. Finally, the results of validation tests and the performance of the post-processing technique to remove the effect of AML are presented in Section 4.

2. Proposed method: SHADE

2.1. Ambient light estimation

A spectroscopy device usually contains a light source with either continuous spectral or several light-emitting diodes (LEDs). In

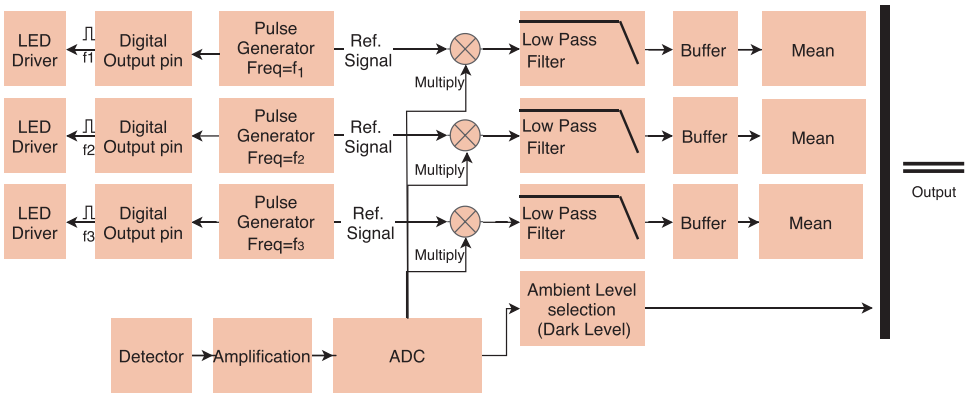

Fig. 1. The structure of the program inside the MCU as an example of SHADE implementation.

the latter, these components are controlled by "LED drivers" (Fig. 1.) The LED driver S_k controls the LED states as it turns-on ($S_k = 1$) or turns-off ($S_k = 0$). S_k is a function with respect to time t, period T_k, and turn-on duration d_k given by

$$S_k(t;\, d_k,\, T_K) = \begin{cases} 1 & d_k \le t \bmod T_k \\ 0 & \text{otherwise} \end{cases} \tag{1}$$

In a multi-wavelength spectroscopy device, the N target wavelengths are regulated by the N drivers: $S_1, S_2, \ldots, S_N$. Let $D_S(t)$ be the sum of the controllers $D_S(t) \equiv D_S(t; \{d_k, T_K\}_{k=1}^N) = \sum_{k=1}^{N} S_k(t; d_k, T_K)$. Due to the periodicity of each S_k, it is clear that if $\left\{\frac{T_i}{T_j} \in \mathbb{Q} |\ \forall\, i, j \in \{1, 2, \ldots, N\}\right\}$, $D_S(t)$ is a periodic function with period $T_D = \mathrm{LCD}(T_1, T_2, \ldots, T_N)$ where $\mathrm{LCD}(\cdot)$ is the least common denominator. Even though the trajectory of $D_S(t)$ depends on the group of parameters $\{d_k, T_k\}$, it is ensured that $D_S(t) = 0$ when $t \in U_D$:

$$U_D = \cup_{n=1}^{\infty}[n(T_D - z_d),\, nT_D] \tag{2}$$

$$z_d = \min(T_1 - d_1,\, T_2 - d_2, \ldots, T_N - d_N) \tag{3}$$

Since no LED is turned on during this interval, we refer to this lapse of time as "dark period", similarly termed in literature [15,16].

The optical receiver measures the optical signal intensity $Y_A^*(t)$. Due to hardware constraints during the analog-to-digital (ADC) conversion, the true intensity $Y_A^*(t)$ is limited with an upper bound at the maximum ADC output level L_{ADC} before being further processed by the micro-controller. Therefore, the measured signal $Y_A(t)$ can be slightly different to the analog observation. Nevertheless, $Y_A(t)$ can be modeled as a hierarchical structure:

$$Y_A(t) = \max(Y_A^*(t),\, L_{\mathrm{ADC}}) \tag{4}$$

$$Y_A^*(t) = Y_S(t) + \kappa(t)\eta(t) + \varepsilon(t) \tag{5}$$

$$\eta(t) = Y_\eta(t) + I_\eta(t) \tag{6}$$

where T_s is the sampling period of the system, the ambient light $\eta(t)$ is modeled as in [25]: a sum of an additive noise composed of the produced zero-mean interference $Y_\eta(t)$, the discrete direct-current (DC) due to the photocurrent effect $I_\eta(t)$. However, we consider the ALE with a time-varying impact described by $\kappa(t) \ge 0$. The errors produced by the photodiode and ADC are modeled with a white noise as $\varepsilon(t) \sim \mathcal{N}(0, \sigma_\varepsilon^2)$. In contrast with the model of [25], we do not make any further assumptions about the characteristic of $\eta(t)$ but rather its additive property.

The crucial part of the ambient light compensation method is noise reconstruction. It should be noted that in the set $t \in U_D$, $Y_S(t) = 0$, and therefore, $Y_A(t) = \max(\eta(t), L_{\mathrm{ADC}})$. Assuming that the saturation level of the ADC is higher than the maximum amplitude of the noise, $Y_A(t) = \eta(t)$. Thus, we can reconstruct low-frequency noise components sampling every T_D when $t \in U_D$:

$$\tilde{\eta}(t) = \begin{cases} Y_A(t) & t \in U_D \\ \tilde{\eta}(t - T_s) & \text{otherwise} \end{cases} \tag{7}$$

It is worth mentioning that the precision on the sampler for a correct reconstruction is $\frac{1}{2}z_d$.

2.2. Empirical ambient light compensation

In addition to the estimation of the AML signal $\tilde{\eta}(t)$, we also add an efficient empirical compensation algorithm to minimize the effect of the noise. Different methods have been previously developed for acoustic applications with feedforward active noise reduction as: recursive least estimator, Kalman filters, and independent component analysis [26–28]. All are based on the following assumptions: (a) the sources are (statistical) independent with constant effect over time, (b) the noise has a constant linear effect on the signal, or (c) the signals are stationary. None of those conditions can hold in the case of hemodynamic signal measurements: the expected value of the signal follows a pattern described by the convolution of the stimuli and a kernel function known as hemodynamic response function with autocorrelated noise, that will violate the assumptions (b) and (c). Moreover, it is known that light sources can affect only in specific intervals [25], therefore the premises (a) and (b) also cannot be valid. Under these conditions, we provide an computational efficient post-processing algorithm:

1. Detection of intervals impacted by AML. Due to the characteristics of the light sources, we cannot make a general assessment of the shape of $Y_\eta(t)$, and the domain of $I_\eta(t)$. However, we hold the assumption that $\eta^*(t) = 0$ in several portions of the data. This condition allowed us to use sequential change points detection algorithms, such as the method described in [29], or robust time-varying variance estimators [30]. In this paper, we prefer to use change point detection, however due to the natural high amplitude of $I_\eta(t)$, all the methods should conclude with similar results. After detecting those changes, we can split the noise signal into a series of $m + 1$ intervals with the change points at $\{t_{1,c}, t_{2,c}, \ldots, t_{m,c}\}$.
2. For each change point $t_{n,c}$, we define a neighborhood of radius $\mathfrak{N}_{n,c} = \{t_{n,c} - \tau T_s, \ldots, t_{n,c}, \ldots, t_{n,c} + \tau T_s\}$. These sets of points allowed us to obtain a good estimator of the median value at $t_{n,c}$. Now, consider the set of intervals when the noise components are higher than zero: $\mathcal{T} = \{[t_{i,c}, t_{i+1,c}] |\ \exists\ t_k \in [t_{i,c}, t_{i+1,c}],\, \eta^*(t_k) \ne 0\}$. For each interval $T_i = [t_{i,c}, t_{i+1,c}]$ in this set, we use these neighborhoods to construct a trend line $\widetilde{Y}_A(t)$ between the median of $Y_A(t)$ in $\mathfrak{N}_{i,c}$ and $\mathfrak{N}_{i+1,c}$.
3. Assuming that the interval size is reasonably small, $\kappa(t)$ can be considered as a constant, and therefore, the local effect of the noise

$\eta(t)$ in the detrended signal $Y_A(t) - \widetilde{Y}_A(t)$ will be linear:

$$(Y_A(t) - \widetilde{Y}_A(t)) = \alpha_{0,i} + \alpha_{1,i}\eta(t) + \epsilon_i(t) \quad t \in T_i \tag{8}$$

where $\alpha_{0,i}$ is the intercept and $\alpha_{1,i}$ the local impact of the noise at the analyzed interval. This model can be solved with an ordinary least squared method. We let $\epsilon_i(t)$ not to follow a normal distribution, although the coefficients of the model are still minimum-variance unbiased estimators.This formulation allowed $\alpha_{0,i}$ and $\alpha_{1,i}$ to vary over time and the compensation method to address noise effects dynamically.

1 Our estimation of $Y_S(t) + \varepsilon(t)$, $\widehat{Y}_S(t)$, at an interval $\mathcal{T}_i$ is presented as a composition between the median trend $\widetilde{Y}_A(t)$ and the portion of the signal that cannot be directly explained by the ambient light:

$$\widehat{Y}_S(t) = \widetilde{Y}_A(t) + \epsilon_i(t) \quad t \in T_i \tag{9}$$

2.3. Implementation

For implementation and testing, we use digital signal processing (DSP) architecture because it offers better flexibility and stability over analog equivalents. The better flexibility and stability of digital signal processing (DSP) architectures over analog equivalents made them an attractive platform for our experiment.

However, a straightforward implementation could not be directly applied due to the differences in working speed between the electrical modulation and demodulation subsystems (operating frequency is in the range of kilohertz) and the allowed communication speed of the commercial operating systems in personal computers (PC). The low-level hardware gathers the data from an analog-to-digital converter (ADC), and the PC is entitled to store and plot the data. Under these conditions, the DSP should execute all the computations within one sample clock, i.e., in a real-time mode. The lower limit of the sampling clock depends on the signal of interest bandwidth (which in hemodynamics application is below 5 Hz) and the desired modulation frequency. Considering these criteria, an ARM® based 32-bit microcontroller (MCU) with digital signal processing instructions, was programmed. Furthermore, the digital output pins of the MCU drive the LED current sources with square-wave signals, as depicted in Fig. 2. These signals drive the LEDs with wavelengths of 735 nm, 805 nm, 850 nm. (Fig. 1).

The emitted light wavelengths are jointly detected by a detector that works in a broad optical spectrum range. The output of the optical detector is an analog signal, which is formed by overlapping the modulated signals converted from optical to the electrical domain. The analog signal is then digitized with a sampling frequency, which is twice the modulating signal bandwidth. The hardware was designed based on a precise ADC with only one clock cycle of latency. The MCU program multiplies the digitized signal to three reference signals. This multiplication with a set of follow-up low pass filters demodulates each wavelength. The reference signals match the phase of the detected signals to ensure correct demodulation. Furthermore, the demodulated signals are down-sampled with an averaging window of 200 samples to reduce the variance and high-frequency fluctuations. Consequently, the signal-to-noise ratio (SNR) will increase. The obtained signal has a sampling frequency above the hemodynamic signal bandwidth and simultaneously satisfies the communication constraints as previously described.

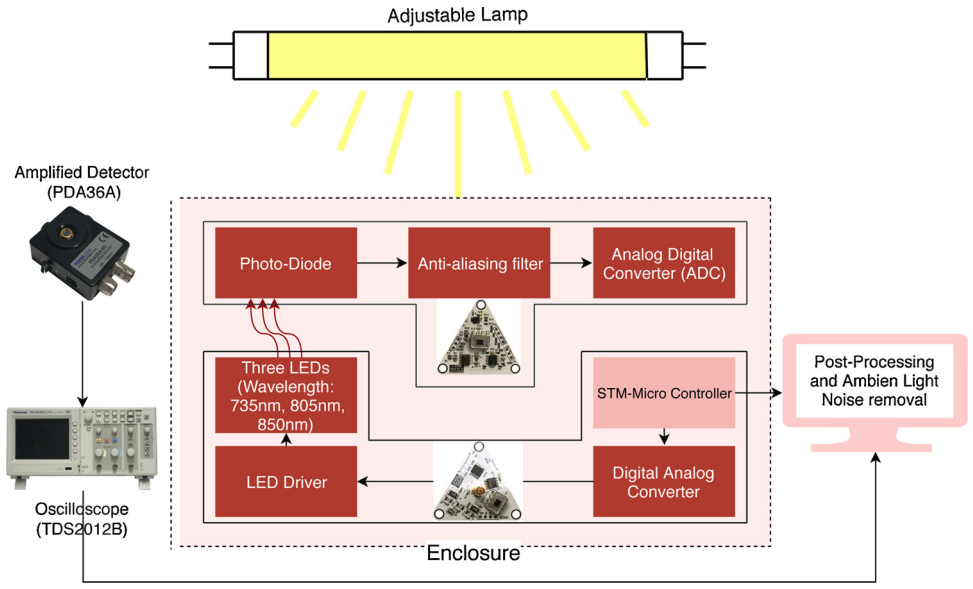

Fig. 2. The first experimental setup to assess the robustness of the implemented SHADE to detect distinct shapes of AML variations.

3. The experimental setup

We tested the proposed technique with two experiments conducted by using the hardware described in Section 2.3. The specific objectives of these tests were to investigate: 1. The strength of the implemented technique in determining distinct shapes of AML variations, 2. The effectiveness of the foam enclosure in dealing with AML. 3. The consequence of SHADE in interpreting physiology data. 4. The potential of the method for AML compensation.

In both trials, an adjustable fluorescent lamp was utilized for variation of AML levels, while a second detection system was measuring AML variation as a control. The reference system was configured based on an amplified detector (PDA36A) connected to an oscilloscope (TDS2012B). A PC recorded the measurements of the oscilloscope and also gathered the data from the DSP board through serial communication (Fig. 1). The discrimination of wavelengths was checked by powering down each wavelength and controlling the amplitude of other wavelengths, separately.

In the first experiment, we investigated the conformity of measured AML with the control setup and its estimation by SHADE implemented in MCU. A lightproof optical enclosure was used to cover the light source, detector, and the DSP board. The coverage attenuates the AML to some extent, which simulates the conditions beyond the laboratory environment. In practical situations, the AML leakage is inevitable as any movement may cause mechanical detachments of the contact surfaces between the cover and the skin. In addition, it is more challenging to design an enclosure that matches the geometry of large body parts such as the human head. The irregular shape and anatomical variation of such a body part would also prevent the profile of surfaces (between the enclosure and the skin) from perfect alignment. Thus, AML leakage is influencing some optical topography devices, even without the effect of motion artifacts.

In another experiment, the hardware was embedded into a foam with a thickness of 5 mm. Then, it was put on to a lower arm to measure the blood flow variation. The test execution also involved AML alteration, as described before. The foam enclosure is an effective solution to partially protect spectroscopy devices from AML [31,32]. This effectiveness is due to their deformability to the surface profile of the skin and the resultant proper surface contact. The appropriate contact reduces AML leakage and also prevents AML from reaching the area under investigation. A pressure cuff was used to partially occlude the blood flow by applying a pressure of 160 mmHg. The pressure ascending period lasts three seconds. In the first part of the trial (0–100 s), the focus was on the evaluation of the system in distinguishing the change in blood flow. In the second part of the test (100–250 s), AML alterations were tested. Fig. 3 represents the experimental setup.

Finally, the mentioned post-processing method to exclude the AML effect (Section 2.2) was applied to the data. However, the necessity of providing AML information and the means for integrating this information with narrow-band detection is the main focus of this paper.

4. Result and discussion

The discrimination of wavelengths was checked by powering down each wavelength and controlling the amplitude of other wavelengths. We did not see any significant change, which agrees with the theoretical expectations presented in Section 2. Fig. 4 presents the time-series output of the DSP and the control setup (PDA36A) from the first experiment. The DSP controlled the LED drivers, sampled the detector output at twice the Nyquist rate, and then demodulated the received signal to wavelength components. The AML associates with AML estimation, and each number represents the LED with peak radiation at that specific optical wavelength. As the upper part of the figure shows, AML measurement by the reference setup is similar to AML estimation by SHADE. This agreement is a verification of the objective of this experiment: SHADE can accurately estimate high time-varying AML. Furthermore, the results also confirm that AML alterations can pollute the signals despite the use of narrow-band detection.

The impact of the first three AML pulses, as well as the one at 160 s, is unnoticeable. This ineffectiveness is due to the low amplitude of AML. In these periods, the narrow-band detection and the enclosure are sufficient enough to eliminate the effect of AML. However, they partially fail to compensate AML with a higher amplitude. This intense AML occurred between 100–140 s and 170–190 s. What stands out in Fig. 4 is the effect of non-homogeneous illumination. This effect is visible in some small fluctuations of AML signals (e.g., between 115–120 s). These oscillations represent small mechanical movements of the AML source. This motion

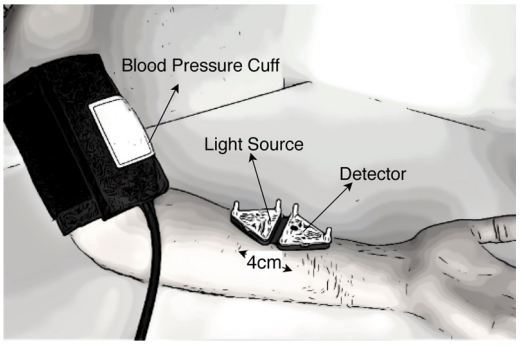

Fig. 3. The experimental setup for SHADE evaluation is depicted. The system is used to detect blood flow variation in the upper arm of a subject.

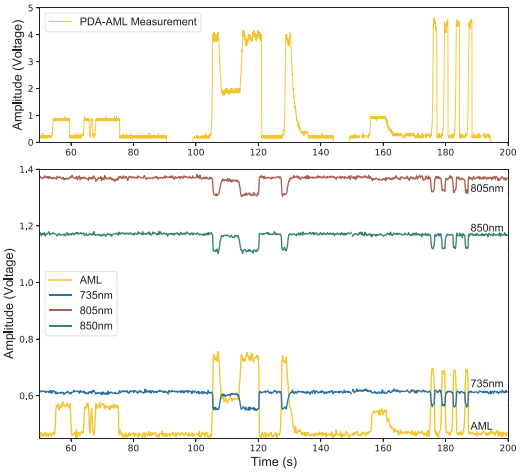

Fig. 4. First experiment results: The output of DSP powered with SHADE (lower section of the graph) and the measurement of the reference amplified detector (upper section). The hemodynamic-related optical signals in the bottom graph, from the lowest to the highest amplitude, are labeled as AML, 735 nm, 850 nm, and 805 nm, respectively.

created by stretching the lamp pull chain to adjust AML. Based on the results, it is logical to conclude SHADE offers not only some degree of compensation but also provides AML information, which may be useful for further recovery of the signal.

Turning to the second experiment, Fig. 5 plots the signals. The partial obstruction of the blood flow occurred in the 20 s and 80 s of the examination. The pressure relief of the cuff happened 20 s afterward. There is a gradual decline in the signal amplitude upon applying pressure. At the release of the force, a sudden fall, then an incremental signal increase is noticeable. This pattern is known as reperfusion hyperamia, and originates from the absorption change of near-infrared light due to blood flow variation [33]. Similar to the first test, AML estimation is identical to the signal measured by the reference. The effect of AML on the result is non-linear and depends on its amplitude.

On the other hand, a surprising aspect of the plots is in the mismatch impact of AML on different wavelengths (Fig. 5). This discrepancy may be the result of inconsistent absorption and scattering of AML while it is traveling through the tissue. The underlying reason for this non-uniformity does not alter the requirement of the provision of AML measurement.

The AML compensation post-processing method described in Section 2.2 and 2.3 managed to alleviate the effect of AML pulses, as depicted in Fig. 6.

There is a performance limitation in identifying AML in a specific range of frequency. The range spans above DC to half of the sampling frequency of dark level measurement. The rate should also be less than the cut-off frequency of the antialiasing filter in the hardware. These conditions rarely happen concurrently. In the implemented program on the customized circuit, this frequency is 83 Hz. This sampling rate is adequate for most of the AML sources such as daylight and fluorescent lamps. However, this will perform

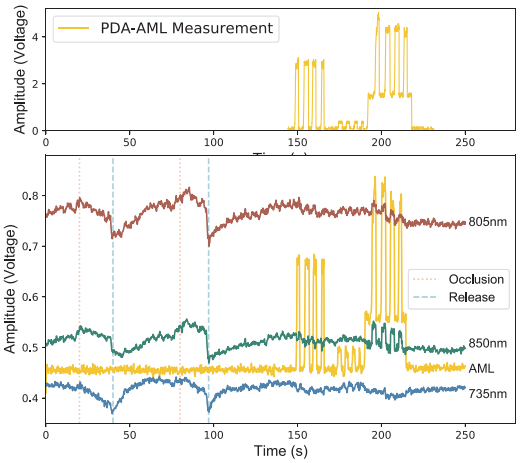

Fig. 5. The output of DSP powered with SHADE (lower section of the graph) and the measurement of the amplified detector (upper section) as a reference in the second experiment (Fig. 3). Partial blood occlusion occurs at 20 and 80 s and the release of the pressure after 20 s. The label scheme is similar to Fig. 4 except for the 735 nm line, which appeared below AML. The lower amplitude of wavelength signals is the result of light absorption by the tissue (the lower arm, as depicted in Fig. 3).

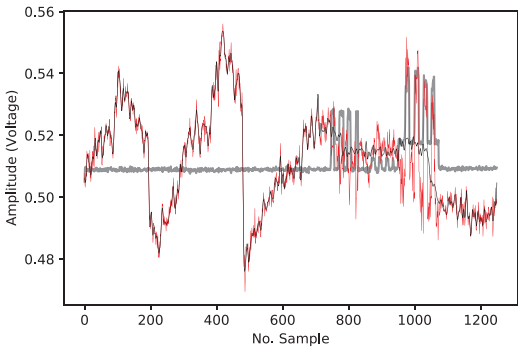

Fig. 6. The visual demonstration of applied post-processing method to alleviate the effect of AML variations. The AML noise is depicted in gray color. The preprocessed and processed signals are red and black, respectively. (For interpretation of the references to color in this figure legend, the reader is referred to the web version of this article.)

inadequately for incandescent light, which oscillates with the frequency of the power line (50 Hz or 60 Hz). The solution may be an alteration of modulating frequencies and should be investigated further.

5. Conclusions

Optical tomography and absorption spectroscopy are restricted due to the negative impact of ambient light (AML). In order to reduce the effects of such a phenomenon and record high-quality optical signals, we have developed a method named SHADE: "absorption spectroscopy enhancement with ambient light estimation and narrow-band detection." The method is constructed on four central concepts: (1) Frequency-division method as a low-noise and noise-robust multiplexing/demultiplexing method for the light wavelengths; (2) Inverse notch filters as a highly robust signal detection technique; (3) Simultaneous AML intensity measurement during "dark moments"; (4) A compensation algorithm for post-processing removal of AML interference.

We have implemented SHADE in an ARM microcontroller and have confirmed the accuracy of the AML measurements under time-varying conditions of an interfering light source using an amplified light detector (PDA36A). The system was further validated based on the hemodynamic response using pressure cuff occlusion. It verified the efficiency of the SHADE to reconstruct the signals when intense AML can distort the biomedical signals.

The jointly signal processing techniques developed and integrated into SHADE is a promising method that will hopefully extend the application of absorption spectroscopy beyond laboratory conditions towards more portable health care applications.

Conflicts of interest

None declared.

Acknowledgement and funding

This work was financially supported by the Research Council of Norway and Oslo Metropolitan University/Faculty of Technology, Art and Design. The funded Project is "Patient-Centric Engineering in Rehabilitation (PACER)" and project No. is 273599.

References

[1] S.J. Carey, H. McCann, F. Hindle, K. Ozanyan, D. Winterbone, E. Clough, Chemical species tomography by near infra-red absorption, Chem. Eng. J. 77 (2000) 111–118, https://doi.org/10.1016/S1385-8947(99)00139-4.
[2] H. Jiang, Diffuse Optical Tomography: Principles and Applications, CRC Press, 2018.
[3] I. Giannini, M. Ferrari, A. C. de Resmini, P. Fasella, Multiple wavelength light photometer for non-invasive monitoring, 1992. US Patent 5,088,493.
[4] T. Durduran, R. Choe, W.B. Baker, A.G. Yodh, Diffuse optics for tissue monitoring and tomography, Rep. Prog. Phys. 73 (2010) 76701.
[5] Y. Chen, B. Kateb, Neurophotonics and Brain Mapping, CRC Press, 2017.
[6] Y. Mendelson, A.C. Clermont, R.A. Peura, B.-C. Lin, Blood glucose measurement by multiple attenuated total reflection and infrared absorption spectroscopy, IEEE Trans. Biomed. Eng. 37 (1990) 458–465.
[7] R.R. Fluck, C. Schroeder, G. Frani, B. Kropf, B. Engbretson, Does ambient light affect the accuracy of pulse oximetry? Respir. Care 48 (2003) 677–680.
[8] H. Sherkat, T. Gjvaag, P. Mirtaheri, Experimental investigation on the light transmission of a textile-based over-cap used in functional near-infrared spectroscopy, European Conference on Biomedical Optics, Optical Society of America (2019) p. 11074_70.
[9] Y. Hoshi, M. Shimada, C. Sato, Y. Iguchi, Reevaluation of near-infrared light propagation in the adult human head: implications for functional near-infrared spectroscopy, J. Biomed. Optics 10 (2005) 64032.
[10] F. Chenier, M. Sawan, A new brain imaging device based on fnirs, 2007 IEEE Biomedical Circuits and Systems Conference, IEEE, 2007, pp. 1–4.
[11] R.D. Frostig, In Vivo Optical Imaging of Brain Function, CRC Press, 2009.
[12] P. Pinti, C. Aichelburg, S. Gilbert, A. Hamilton, J. Hirsch, P. Burgess, I. Tachtsidis, A review on the use of wearable functional near-infrared spectroscopy in naturalistic environments, Jpn. Psychol. Res. 60 (2018) 347–373.
[13] D.T. Delpy, M. Cope, P. van der Zee, S. Arridge, S. Wray, J. Wyatt, Estimation of optical pathlength through tissue from direct time of flight measurement, Phys. Med. Biol. 33 (1988) 1433.

[14] S.-H. Lee, Reducing the effects of ambient noise light in an indoor optical wireless system using polarizers, Microw. Opt. Technol. Lett. 40 (2004) 228–231.
[15] AFE4403 Ultra-Small, Integrated Analog Front-End for Heart Rate Monitors and Low-Cost Pulse Oximeters, Texas Instruments, 2014 Rev. B..
[16] AFE4490, Integrated Analog Front-End for Pulse Oximeters, Texas Instruments, 2012 Rev. H..
[17] M.A. Khalil, H.K. Kim, I.-K. Kim, M. Flexman, R. Dayal, G. Shrikhande, A.H. Hielscher, Dynamic diffuse optical tomography imaging of peripheral arterial disease, Biomed. Optics Express 3 (2012) 2288–2298.
[18] M.G. Ruppert, D.M. Harcombe, M.R. Ragazzon, S.R. Moheimani, A.J. Fleming, A review of demodulation techniques for amplitude-modulation atomic force microscopy, Beilstein J. Nanotechnol. 8 (2017) 1407–1426.
[19] A. von Lühmann, H. Wabnitz, T. Sander, K.-R. Müller, M3ba: a mobile, modular, multimodal biosignal acquisition architecture for miniaturized eeg-nirs-based hybrid bci and monitoring, IEEE Trans. Biomed. Eng. 64 (2016) 1199–1210.
[20] S. Coyle, T. Ward, C. Markham, G. McDarby, On the suitability of near-infrared (nir) systems for next-generation brain-computer interfaces, Physiol. Meas. 25 (2004) 815.
[21] M. Kiguchi, H. Atsumori, I. Fukasaku, Y. Kumagai, T. Funane, A. Maki, Y. Kasai, A. Ninomiya, Note: wearable near-infrared spectroscopy imager for haired region, Rev. Sci. Instrum. 83 (2012) 56101.
[22] S.K. Piper, A. Krueger, S.P. Koch, J. Mehnert, C. Habermehl, J. Steinbrink, H. Obrig, C.H. Schmitz, A wearable multi-channel fnirs system for brain imaging in freely moving subjects, Neuroimage 85 (2014) 64–71.
[23] G. Bauernfeind, R. Leeb, S.C. Wriessnegger, G. Pfurtscheller, Development, set-up and first results for a one-channel near-infrared spectroscopy system/entwicklung, aufbau und vorläufige ergebnisse eines einkanal-nahinfrarot-spektroskopie-systems, Biomed. Tech. 53 (2008) 36–43.
[24] J.M. Masciotti, J.M. Lasker, A.H. Hielscher, Digital lock-in detection for discriminating multiple modulation frequencies with high accuracy and computational efficiency, IEEE Trans. Instrum. Meas. 57 (2007) 182–189.
[25] A. Moreira, R. Valadas, A. de Oliveira Duarte, Performance of infrared transmission systems under ambient light interference, IEE Proc.-Optoelectron. 143 (1996) 339–346.
[26] N.V. George, G. Panda, Advances in active noise control: a survey, with emphasis on recent nonlinear techniques, Signal Process. 93 (2013) 363–377.
[27] L. Luo, J. Sun, B. Huang, D.D. Quoc, Efficient combination of feedforward and feedback structures for nonlinear narrowband active noise control, Signal Process. 128 (2016) 494–503.
[28] C.D. Petersen, R. Fraanje, B.S. Cazzolato, A.C. Zander, C.H. Hansen, A kalman filter approach to virtual sensing for active noise control, Mech. Syst. Signal Process. 22 (2008) 490–508.
[29] D.M. Hawkins, Q. Deng, A nonparametric change-point control chart, J. Qual. Technol. 42 (2010) 165–173.
[30] L. Zhang, Y. Guan, Variance estimation over sliding windows, Proceedings of the Twenty-Sixth ACM SIGMOD-SIGACT-SIGART Symposium on Principles of Database Systems, ACM, 2007, pp. 225–232.
[31] F. Orihuela-Espina, D.R. Leff, D.R. James, A.W. Darzi, G.-Z. Yang, Quality control and assurance in functional near infrared spectroscopy (fnirs) experimentation, Phys. Med. Biol. 55 (2010) 3701.
[32] A. Bozkurt, A. Rosen, H. Rosen, B. Onaral, A portable near infrared spectroscopy system for bedside monitoring of newborn brain, Biomed. Eng. Online 4 (2005) 29.
[33] R. Kragelj, T. Jarm, T. Erjavec, M. Prešern-Štrukelj, D. Miklavčič, Parameters of postocclusive reactive hyperemia measured by near infrared spectroscopy in patients with peripheral vascular disease and in healthy volunteers, Ann. Biomed. Eng. 29 (2001) 311–320.